Alpha track shape analysis for different sources ^{239}Pu, ^{210}Po and ^{241}Am using CR-39 SSNTD.

H. A. S. Aly

Physics Department, University College for Women, for Arts, Science and Education, Ain Shams University, Cairo, Egypt.
Hanan_ali2@women.asu.edu.eg

Abstract: Quantitative and qualitative analysis of alpha tracks porfile using CR-39 irradiated by collimated alpha beam have been investigated for different alpha sources namely ^{239}Pu, ^{241}Am and ^{210}Po. Alpha track shape characteristics have been studied and the dependence of track minor and major axes and depth as well as track density on detector to source spacing is investigated. It was found that major and minor axes become nearly identical i.e. the track base shape changes from ellipse to be a circle at alpha source detector spacing $x_c \approx 22$ mm. for ^{239}Pu, 26 mm. for ^{210}Po and 30mm. for ^{241}Am. Alpha range in air has been also determined.
[H. A. S. Aly **Alpha track shape analysis for different sources ^{239}Pu, ^{210}Po and ^{241}Am using CR-39 SSNTD.** *Life Sci J* 2013;10(2):1909-1920] (ISSN: 1097-8135). http://www.lifesciencesite.com. 268

Keywords: Alpha track, CR-39, ^{239}Pu, ^{241}Am , ^{210}Po

1.Introduction:

Fast heavy charged particles (like alpha particles and other light ions etc.) create latent tracks in some dielectric materials. After chemical etching in aqueous NaOH or KOH solutions, these tracks become visible under an optical microscope **[Nikezic *et al*., 2006]**.

The diameter of α-particles track in CR-39 can be used as a measure of α-particle energy, provided that the α-tracks are etched to the end of their respective range: The diameter is found to be high for large residual energies, and low for small energies [**Khayrat *et al*., 1999]**.

When a charged particle traverses inside CR-39, it leaves behind an ionization trail that is more sensitive to chemical etching than the rest of the bulk. Upon treatment with a chemical etching agent, tracks remain as holes or pits, by measuring the size of the track; it should be possible to identify the particle that created the track and to determine its energy **[Mosier, 2009].**

Because of their double-positive charge, alpha particles have great ionizing power, but their large mass results in very little penetration. For example, alpha particles from 4 to 10 MeV have ranges in air of 5–11 cm **[Bobby, 2005]**.

2. Methodology:

In the present work, Track diameter as well as the major and minor axes, track density and alpha range were measured for ^{239}Pu, ^{210}Po and ^{241}Am using CR-39 type Solid State Nuclear Track Detector (SSNTD) films.

CR-39 detectors under normal incidence through a collimator were irradiated with alpha particles with maximum initial incident energy of 5.1, 5.4, 5.5 MeV from planer alpha sources ^{239}Pu, ^{210}Po and ^{241}Am respectively, were studied. The used detectors were cut to a size of 1cm^2. Effect of air spacing between detector and alpha source was intended in the present study to control the final alpha energies incident on the detector. Relationship between the alpha track profile and the air distance travelled by an alpha particle for different sources was therefore needed. Setup of CR-39 alpha irradiation process is display in Fig.1

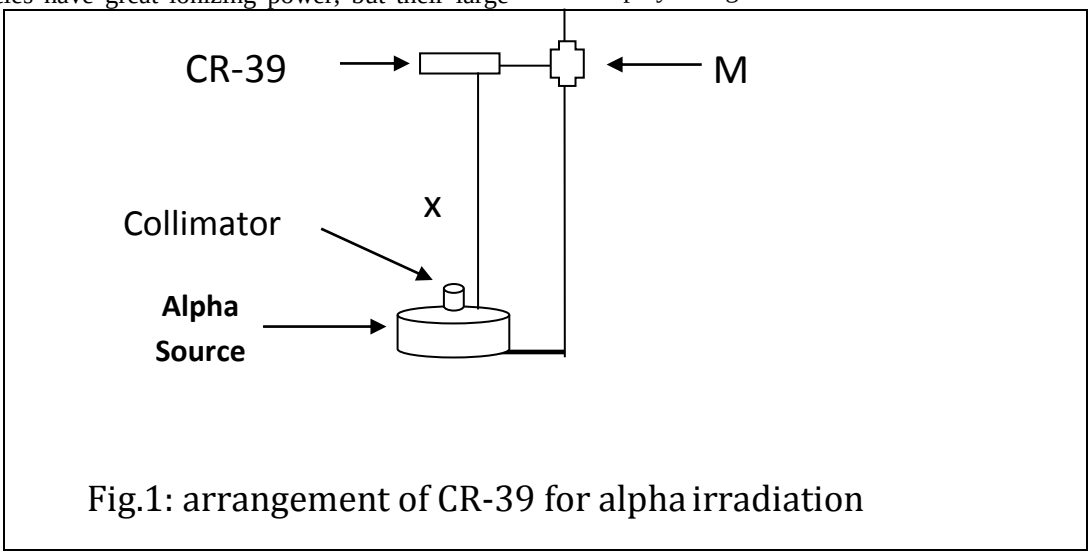

Fig.1: arrangement of CR-39 for alpha irradiation

Movable holder M has been used to changes detector to alpha source space distance x, alpha beam will travel to detector after collimation. Collimator of height 2 mm was placed bounded to alpha source, CR-39 detectors after preparations were holed such that one side of it faced to the alpha source and parallel to its plane to insure normal incidence of alpha beam on the detector surface which irradiated for 3 min. Immediately after irradiation, the detectors were etched in a 6.25 N aqueous solution of NaOH maintained at 70 $\pm$ 1C^{o} in a water bath. If the etching time keeps on increasing, the diameters of the tracks also keep on increasing, but their relationship to the energy of the incident particles is lost **[Espinosa, 1998]**. The correct etching time must be short enough to avoid over etched tracks, but long enough to have track wide enough for the image analysis **[Caresana *et al.*, 2012]** also to reduce recorded tracks shortness 3 h was chosen etching time in the present study,. The detectors were then taken out from the etchant, rinsed with distilled water and dried in air. A piece of etched detector (with the alpha tracks) was then placed inside the mould on the bottom, with the side containing the tracks facing upwards. The track density is counted manually for a number of 100 fields of view. The number of tracks per cm^2 is then calculated using a calibration factor which converts the number of tracks observed directly per unit area.

The area of one field of view was calculated by a stage eyepiece and the track density was calculated in terms of tracks per cm^{-2}, the background track density was determined by processing a virgin detector under the same etching conditions, then background was subtracted from the measured track density, in order to obtain realistic statistics of the tracks. The calibration factor of 0.18 ± 0.002 tracks cm^{-2}, obtained from an earlier calibration experiment for the (CR-39) track detector **[Khan *et al.*, 1990].**

The resolution of the general optical microscope is around 0.3 μm, so the error will become larger than 10% for tracks shorter than 3 □m **[Ng *et al.*, 2007]**, in the present study the recorded tracks have minimum depth exceed this value.

The track density T can be calculated from the following relation

$$T = \frac{N - N_B}{SM} \qquad (1)$$

Where; N, N_B, M and S are the number of tracks, number of background's tracks, field number and area of view, respectively.

3. Results and Discussion:

Recorded track for different alpha emitters have been investigated and the values of minor a, major axes b and track depth d have been measured for different tracks. Track parameters (a, b and d in □m) for five tracks with largest depths for each source to detector spacing, these track were have minimum values of minor and major axes have been selected and are listed in Tables.1,2 &3 for ^{239}Pu, Tables.4,5& 6 for ^{210}Po and finally Tables.7,8 &9 for ^{241}Am.

Figs.2, 3 and 4 displays the trend of average values of minor axis a, major axis b and depth d as a function of source to detector spacing x for different studied alpha emitters.

Dependences of a, b and d (μm) on x (mm), with regardless to the end point where alpha straggling affect on the produced diameters, are given in the following equation groups:

First group display minor axis values as a function in x for ^{239}Pu, ^{210}Po and ^{241}Am respectively.

$$\begin{Bmatrix} a(^{239}Pu) = 0.163x + 0.770 \\ a(^{210}Po) = 0.14x + 0.705 \\ a(^{241}Am) = 0.134x + 0.695 \end{Bmatrix} \qquad (2)$$

Second group display major axis values as a function in x for ^{239}Pu, ^{210}Po and ^{241}Am respectively.

$$\begin{Bmatrix} b(^{239}Pu) = 0.126x + 1.983 \\ b(^{210}Po) = 0.108x + 1.750 \\ b(^{241}Am) = 0.102x + 1.724 \end{Bmatrix} \qquad (3)$$

Third group display depth values as a function in x for ^{239}Pu, ^{210}Po and ^{241}Am respectively.

$$\begin{Bmatrix} d(^{239}Pu) = -0.012x^2 + 0.028x + 21.32 \\ d(^{210}Po) = -0.014x^2 + 0.022x + 24.71 \\ d(^{241}Am) = -0.015x^2 + 0.019x + 25.8 \end{Bmatrix} \qquad (4)$$

Each group of equations has been treated to find the x coefficients as a function of maximum isotope alpha energy Eα, this led to:

$$a = (-0.073E\alpha\ 0.537)\ x + -0.194\ E\alpha + 1.759 \qquad (5)$$

$$b = (= -0.06\ E\alpha + 0.432)\ x + = -0.677\ E\alpha + 5.431 \qquad (6)$$

$$d = (-0.007\ E\alpha + 0.025)\ x^2 + (-0.021\ E\alpha + 0.139)\ x + 11.22\ E\alpha - 35.91 \qquad (7)$$

Eq.4, 6 and 7 shows that minor axis and major axis decreased as alpha particles incident energy increased and as alpha traveling distance in air increased but obtained results of eq.7 shows that track depth will increase as Eα and decreased as alpha travels distance increased this due to the energy loss of alpha particles in air, i.e energy of alpha particles will be deposit in air and CR-39. Recorded track in CR-39 is due to alpha particles reached to it with residual energy dependent on the travel distance in air. Surface density travelled by alpha particles in air and CR-39 for different sources have calculated and listed in Table.10.

Total volume of alpha track produced at different source to detector spacing for different alpha emitters were calculated and listed in Table.11. Fig.5 display the variation of recorded track volume vs alpha travelling distance for ^{239}Pu,

^{210}Po and ^{241}Am. Shown curve is similar to the alpha particles energy loss rate curve [**Khayrat, 1999, Lounits, 2001].**i.e the energy loss may be represented by the produced track volume, Taking into account that the direction of increasing the distance will corresponds to the energy decrease in this direction, where the energy decreased as the distance from the source increased **[Espinosa *et al.*, 2001]**.

For incident angles larger than 60◦, the tracks are almost always circular in shape regardless of the incident energy [**Nikezic *et al.*, 2003]**. Many authors interested only to study circular tracks and avoids non perpendicular incidence of alpha particles **[Espinosa *et al.*, 2001, Ameroa, 2001, Nikezic *et al.*, 2003,],** in the present study the observed tracks had ellipse base till certain distance departing the source from detector after which the tracks became circular. It was found that the distance at which the tracks starting to be circular, which corresponding to perpendicular incidence of alpha particles, dependent on emitter maximum energy. Ratio of major to minor axes was calculated at different source to detector spacing for different alpha emitters and listed in Table.12.

Figs.6.a, b and c show the variation of major to minor axis b/a ratio vs source to detector spacing x for ^{239}Pu, ^{210}Po and ^{241}Am. From Fig.6 the major and minor start to become identical and i.e track become circular at certain value of source to detector spacing was $x_c \approx$ 22 mm. for ^{239}Pu, 26 mm. for ^{210}Po and 30mm. for ^{241}Am.

Total surface density travelled by alpha particles has been calculated and listed in Table.13. After x= 40 mm no recorded tracks have been observed than background and the alpha range for different studied sources calculated from Table.13; were 5.39, 5.502 and 5.543 mg/ cm^3 equivalent to 4.553, 4.65 and 4.68 cm in air, for ^{239}Pu, ^{210}Po and ^{241}Am respectively. These range values comparable to the following equation:

R = 0.321 E□ + 2.910 (8)

Track density for different alpha emitters is listed in Table. 14, as shown in the table the track density decreased as source to detector decreased, no recorded tracks for x > 40 mm.

Fig.7 display track density vs source to detector spacing for different alpha emitters, as shown in the figure track density exponentially decreased as x increased.

Conclusions:

This study intends to layout alpha track shape by qualitative and quantitative analyses for CR-39 recorded track due to alpha irradiation from three different alpha emitters at different source to detector spacing. It was found that the track minor and major axes increased, while track depth was decreased as the source departing from the detector, this due to energy loss in air.

Track shape also affected by source's departing distance from the detector where the track shape changes from elliptical to circular at certain distance dependent on alpha emitter maximum energy.

Variation of track volume is similar to energy loss d*E*/d*x* i.e track volume vs alpha travelled distance curve may represent the energy loss curve with regard that increasing distance equivalent to decreasing energy.

Track density for the different alpha sourced are decreased as alpha travelled distance is increased, where only the maximum alpha energy will be continued reach to detector until its range.

Whole alpha range, surface density penetrated by alpha particles, in air and CR-39 at the same time is calculated for different studied alpha sources

Table.1: minor axis at different heights of source to CR-39 detector for 239Pu.

x(mm)	a1	a 2	a 3	a 4	a 5	Average a (□m)
6	1.42	1.38	1.34	1.36	1.41	1.38
8	1.51	1.46	1.44	1.45	1.51	1.47
10	1.76	1.66	1.71	1.65	1.65	1.69
12	1.95	1.96	1.90	1.90	1.92	1.92
14	2.05	2.04	2.05	2.06	1.90	2.02
16	2.20	2.05	2.34	2.05	2.20	2.17
18	2.78	2.63	2.49	2.63	2.78	2.66
20	2.93	2.93	2.93	3.07	3.22	3.01
22	3.38	3.22	3.20	3.36	3.31	3.29
24	3.46	3.45	3.51	3.50	3.46	3.47
26	3.66	3.72	3.65	3.60	3.73	3.67
28	3.94	3.94	3.83	3.91	3.87	3.89
30	4.10	3.98	3.89	3.95	3.94	3.97
32	4.38	4.47	4.43	4.46	4.35	4.41
34	4.51	4.54	4.54	4.56	4.61	4.55
36	4.71	4.76	4.72	4.66	4.75	4.72
38	4.90	4.84	4.91	4.83	4.87	4.87

Table. 2: major axis at different heights of source to CR-39 detector for ^{239}Pu.

x(mm)	b_1	b_2	b_3	b_4	b_5	Average b (□m)
6	2.15	2.11	2.12	2.14	2.16	2.13
8	2.25	2.23	2.18	2.19	2.22	2.21
10	2.41	2.48	2.40	2.35	2.36	2.40
12	2.59	2.55	2.57	2.52	2.56	2.56
14	2.62	2.60	2.61	2.65	2.67	2.63
16	2.71	2.70	2.76	2.72	2.74	2.72
18	2.98	2.83	2.91	3.01	2.98	2.94
20	3.00	3.06	3.09	3.11	3.08	3.07
22	3.26	3.24	3.27	3.24	3.31	3.26
24	3.53	3.57	3.56	3.53	3.54	3.54
26	3.71	3.67	3.70	3.76	3.74	3.71
28	3.92	3.96	3.92	3.95	3.89	3.93
30	4.01	4.05	3.97	3.99	3.96	3.99
32	4.44	4.51	4.49	4.54	4.55	4.50
34	4.59	4.60	4.61	4.56	4.58	4.58
36	4.72	4.76	4.74	4.70	4.76	4.73
38	4.86	4.88	4.91	4.89	4.84	4.87
40	8.44	8.64	8.47	8.56	8.43	8.51

Table. 3: track depth at different heights of source to CR-39 detector for ^{239}Pu.

x(mm)	d_1	d_2	d_3	d_4	d_5	Average d (□m)
6	20.88	20.71	20.82	20.81	21.25	20.89
8	20.22	20.61	20.41	21.13	20.18	20.51
10	19.28	20.19	20.75	20.81	20.48	20.30
12	20.97	19.75	19.93	20.49	19.85	20.20
14	18.96	19.28	19.61	19.55	19.13	19.30
16	18.73	19.04	18.72	18.92	18.67	18.82
18	17.29	17.51	17.99	17.66	17.29	17.55
20	16.89	16.09	17.25	16.65	16.39	16.65
22	15.13	15.33	15.45	15.67	15.33	15.38
24	14.81	14.78	14.89	14.83	14.92	14.85
26	13.91	13.98	14.01	13.88	13.96	13.95
28	12.67	12.71	12.71	12.69	12.73	12.70
30	10.98	11.07	10.88	11.17	11.08	11.04
32	7.87	7.91	7.84	7.96	7.85	7.89
34	6.62	6.68	6.71	6.59	6.66	6.65
36	5.41	5.29	5.33	5.38	5.37	5.36
38	5.31	5.33	5.18	5.09	5.22	5.23
40	5.18	5.03	4.98	4.88	4.91	5.00

Table.4: minor axis at different heights of source to CR-39 detector for ^{210}Po.

x(mm)	a_1	a_2	a_3	a_4	a_5	Average a (□m)
6	1.60	1.61	1.59	1.58	1.60	1.59
8	1.76	1.81	1.80	1.78	1.81	1.79
10	2.04	1.99	2.03	2.00	2.01	2.01
12	2.22	2.28	2.19	2.20	2.22	2.22
14	2.35	2.33	2.52	2.40	2.42	2.40
16	2.69	2.68	2.65	2.67	2.65	2.66
18	3.06	3.04	3.06	3.05	3.02	3.04
20	3.34	3.44	3.36	3.35	3.31	3.36
22	3.78	3.82	3.80	3.85	3.78	3.80
24	4.05	4.06	4.09	4.07	4.11	4.08
26	4.35	4.36	4.33	4.36	4.39	4.36
28	4.55	4.56	4.58	4.58	4.58	4.57
30	4.96	4.95	4.91	4.83	4.84	4.90
32	5.12	5.09	5.07	5.08	5.11	5.09
34	5.22	5.29	5.22	5.25	5.28	5.25
36	5.39	5.45	5.42	5.38	5.41	5.41
38	5.51	5.52	5.54	5.54	5.48	5.52
40	8.52	8.55	8.54	8.56	8.50	8.53

Table. 5: major axis at different heights of source to CR-39 detector for ^{210}Po.

x(mm)	b_1	b_2	b_3	b_4	b_5	Average b (□m)
6	2.44	2.43	2.41	2.40	2.40	2.42
8	3.04	2.55	2.56	2.52	2.54	2.64
10	2.76	2.74	2.75	2.72	2.79	2.75
12	2.96	2.94	2.93	2.96	2.91	2.94
14	3.00	3.02	3.04	3.09	3.06	3.04
16	3.11	3.16	3.15	3.14	3.16	3.14
18	3.39	3.37	3.41	3.40	3.42	3.40
20	3.83	3.76	3.75	3.79	3.81	3.79
22	4.05	4.07	4.05	4.07	4.09	4.06
24	4.32	4.25	4.30	4.28	4.27	4.28
26	4.44	4.36	4.33	4.37	4.41	4.38
28	4.53	4.53	4.50	4.54	4.57	4.53
30	4.90	4.89	4.86	4.91	4.83	4.88
32	5.08	5.03	5.05	5.08	5.06	5.06
34	5.20	5.22	5.25	5.26	5.27	5.24
36	5.37	5.38	5.41	5.39	5.35	5.38
38	5.55	5.50	5.45	5.54	5.51	5.51
40	8.76	8.79	8.75	8.81	8.84	8.79

Table. 6: track depth at different heights of source to CR-39 detector for ^{210}Po.

x(mm)	d_1	d_2	d_3	d_4	d_5	Average d (□m)
6	24.29	24.33	24.36	24.51	24.62	24.42
8	23.89	24.09	23.96	24.21	24.04	24.04
10	23.08	22.95	23.04	23.15	22.89	23.02
12	22.51	22.63	22.49	22.62	22.71	22.59
14	22.19	22.31	22.34	22.21	22.17	22.24
16	21.66	21.76	21.83	21.67	21.81	21.75
18	20.41	20.44	20.29	20.36	20.41	20.38
20	19.71	19.64	19.57	19.49	19.63	19.61
22	17.98	18.02	18.06	17.88	18.11	18.01
24	17.35	17.39	17.36	17.29	17.44	17.37
26	16.44	16.51	16.38	16.27	16.29	16.38
28	14.91	14.86	15.08	14.87	15.01	14.95
30	11.09	11.18	11.27	11.33	11.26	11.23
32	9.25	9.23	9.23	9.27	9.21	9.24
34	7.89	7.88	7.92	7.84	8.02	7.91
36	6.33	6.58	6.47	6.39	6.48	6.45
38	6.08	6.14	6.16	6.11	6.08	6.11
40	5.82	5.93	5.91	5.72	5.88	5.85

Table.7: minor axis at different heights of source to CR-39 detector for ^{241}Am.

x(mm)	a_1	a_2	a_3	a_4	a_5	Average a (□m)
6	1.69	1.68	1.64	1.64	1.68	1.67
8	1.91	1.91	1.83	1.84	1.90	1.88
10	2.14	2.10	2.07	2.07	2.09	2.09
12	2.34	2.37	2.29	2.30	2.32	2.32
14	2.48	2.47	2.47	2.49	2.45	2.54
16	2.81	2.79	2.83	2.74	2.79	2.79
18	3.20	3.21	3.22	3.19	3.22	3.20
20	3.54	3.54	3.54	3.56	3.54	3.54
22	3.90	3.83	3.84	3.91	3.86	3.87
24	4.11	4.13	4.16	4.11	4.10	4.12
26	4.34	4.34	4.36	4.44	4.31	4.36
28	4.72	4.74	4.76	4.74	4.74	4.74
30	4.96	4.94	4.99	4.95	4.96	4.96
32	5.44	5.38	5.35	5.39	5.35	5.38
34	5.54	5.56	5.54	5.52	5.60	5.55
36	5.69	5.71	5.71	5.67	5.71	5.70
38	5.92	5.90	5.83	5.84	5.81	5.86
40	9.17	9.19	9.18	9.21	9.15	9.18

Table.8: major axis at different heights of source to CR-39 detector for ^{241}Am.

x(mm)	b_1	b_2	b_3	b_4	b_5	Average b (□m)
6	2.55	2.56	2.54	2.56	2.55	2.55
8	2.67	2.69	2.61	2.64	2.65	2.65
10	2.91	2.94	2.91	2.86	2.90	2.90
12	3.09	3.05	3.08	3.07	3.07	3.07
14	3.16	3.15	3.13	3.17	3.20	3.16
16	3.25	3.33	3.31	3.26	3.28	3.28
18	3.60	3.55	3.56	3.59	3.58	3.57
20	3.94	3.96	3.88	3.92	3.96	3.93
22	4.22	4.26	4.27	4.24	4.22	4.24
24	4.47	4.46	4.44	4.51	4.48	4.47
26	4.60	4.61	4.59	4.62	4.63	4.61
28	4.72	4.77	4.75	4.73	4.74	4.74
30	5.12	5.15	5.09	5.13	5.11	5.12
32	5.31	5.34	5.30	5.36	5.33	5.33
34	5.51	5.52	5.56	5.53	5.52	5.53
36	5.65	5.68	5.70	5.71	5.64	5.67
38	5.83	5.75	5.80	5.86	5.81	5.81
40	9.20	9.26	9.22	9.24	9.29	9.24

Table. 9: track depth at different heights of source to CR-39 detector for ^{241}Am.

x(mm)	d_1	d_2	d_3	d_4	d_5	Average d (□m)
6	25.33	25.27	25.38	25.51	25.92	25.48
8	24.88	25.14	25.09	25.55	24.92	25.12
10	23.88	23.91	23.96	24.11	23.95	23.96
12	23.31	23.53	23.48	23.61	23.58	23.50
14	23.16	23.18	23.09	23.31	23.31	23.21
16	22.71	22.67	22.84	22.72	22.67	22.72
18	21.17	21.29	21.22	21.18	21.13	21.20
20	20.60	20.44	20.33	20.51	20.39	20.45
22	18.73	18.77	18.85	18.88	18.75	18.80
24	18.07	18.03	18.17	18.09	18.04	18.08
26	17.02	17.06	17.11	16.88	17.03	17.02
28	15.46	15.66	15.51	15.63	15.44	15.54
30	11.45	11.76	11.78	11.89	11.68	11.71
32	9.64	9.72	9.56	9.61	9.58	9.62
34	8.19	8.27	8.34	8.17	8.22	8.24
36	6.64	6.88	6.71	6.56	6.83	6.72
38	6.49	6.44	6.29	6.24	6.33	6.36
40	6.29	6.18	6.11	6.22	6.03	6.17

Table.10.total surface area penetrated by alpha particles for different alpha emitters.

x(mm)	S (mg/ cm2)		
	^{239}Pu	^{210}Po	^{241}Am
6	3.448	3.910	4.049
8	3.634	4.096	4.237
10	3.844	4.200	4.323
12	4.067	4.380	4.499
14	4.186	4.571	4.698
16	4.359	4.743	4.871
18	4.430	4.801	4.908
20	4.549	4.936	5.047
22	4.620	4.964	5.067
24	4.786	5.116	5.210
26	4.905	5.224	5.308
28	4.979	5.273	5.351
30	4.997	5.022	5.086
32	4.822	4.999	5.049
34	4.897	5.062	5.104
36	4.964	5.107	5.143
38	5.183	5.300	5.332
40	5.390	5.502	5.543

Table.11 calculated track volume for different alpha emitters.

x(mm)	V $(\mu m)^3$		
	^{239}Pu	^{210}Po	^{241}Am
6	64.47	98.36	113.23
8	69.92	118.86	125.40
10	85.92	133.10	152.09
12	103.89	154.29	175.70
14	107.20	169.85	189.77
16	116.20	190.57	217.92
18	143.90	220.48	253.91
20	161.04	260.98	298.06
22	172.83	291.22	322.27
24	191.24	317.08	348.38
26	198.83	327.06	357.56
28	203.21	324.28	365.26
30	183.19	281.23	311.06
32	163.99	249.01	288.64
34	145.20	227.60	264.33
36	125.29	196.40	227.43
38	129.78	194.30	226.33
40	381.57	459.46	547.13

Table.12 track major to minor axis ratio for different alpha emitters.

x(mm)	b/a		
	^{239}Pu	^{210}Po	^{241}Am
6	1.54	1.52	1.53
8	1.50	1.47	1.47
10	1.42	1.37	1.39
12	1.33	1.33	1.32
14	1.30	1.27	1.28
16	1.26	1.18	1.18
18	1.10	1.12	1.11
20	1.02	1.13	1.11
22	0.99	1.07	1.10
24	1.02	1.05	1.08
26	1.01	1.01	1.06
28	1.01	0.99	1.00
30	1.01	0.99	1.03
32	1.02	0.99	0.99
34	1.01	1.00	1.00
36	1.00	0.99	1.00
38	1.00	1.00	0.99
40	0.99	1.03	1.01

Table.13 total surface density penetrated by alpha particles for different alpha emitters.

x(mm)	S (mg/ cm^2)		
	^{239}Pu	^{210}Po	^{241}Am
6	3.448	3.910	4.049
8	3.634	4.096	4.237
10	3.844	4.200	4.323
12	4.067	4.380	4.499
14	4.186	4.571	4.698
16	4.359	4.743	4.871
18	4.430	4.801	4.908
20	4.549	4.936	5.047
22	4.620	4.964	5.067
24	4.786	5.116	5.210
26	4.905	5.224	5.308
28	4.979	5.273	5.351
30	4.997	5.022	5.086
32	4.822	4.999	5.049
34	4.897	5.062	5.104
36	4.964	5.107	5.143
38	5.183	5.300	5.332
40	5.390	5.502	5.543

Table.14 track density at different source to detector spacing for different alpha emitters.

x(mm)	T(cm^{-2})		
	^{239}Pu	^{210}Po	^{241}Am
6	4140	712	2876
8	2735	456	1982
10	1423	156	1012
12	1154	124	895
14	988	92	472
16	624	76	287
18	564	51	201
20	404	44	166
22	245	33	112
24	158	21	87
26	132	16	66
28	63	11	43
30	47	9	21
32	30	7	14
34	21	5	9
36	17	4	6
38	13	2	4
40	8	1	3

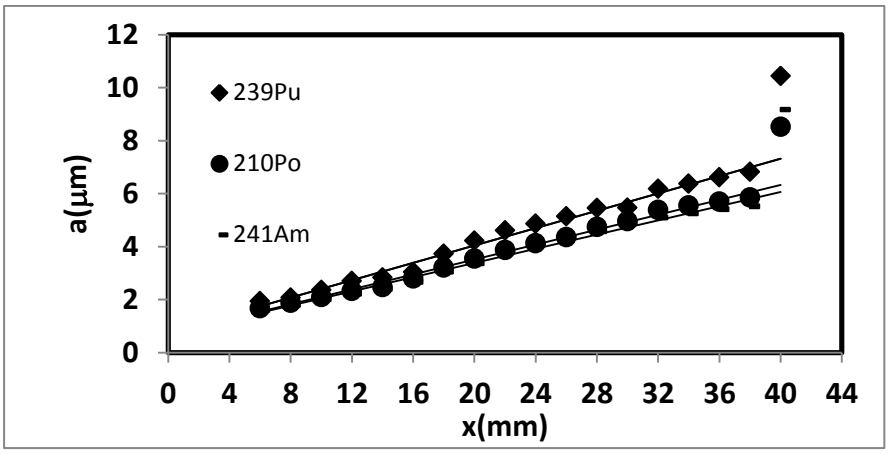

Fig.2 track minor axis at different source to detector spacing for different alpha emitters.

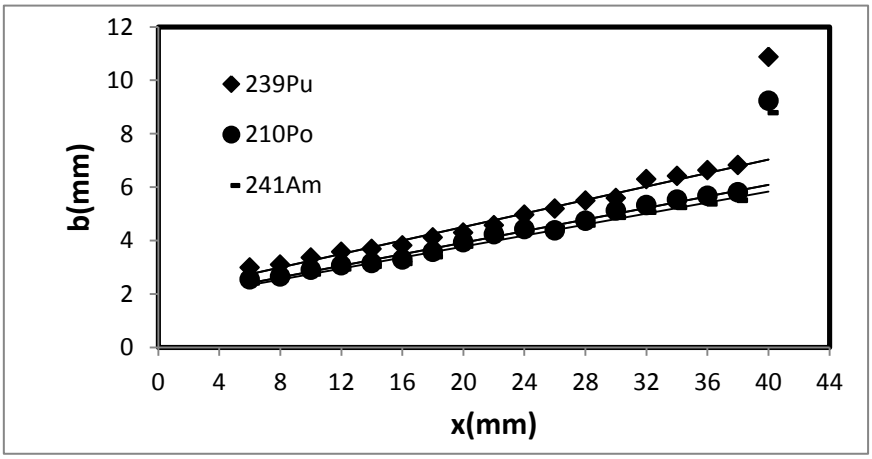

Fig.3 track major axis at different source to detector spacing for different alpha emitters

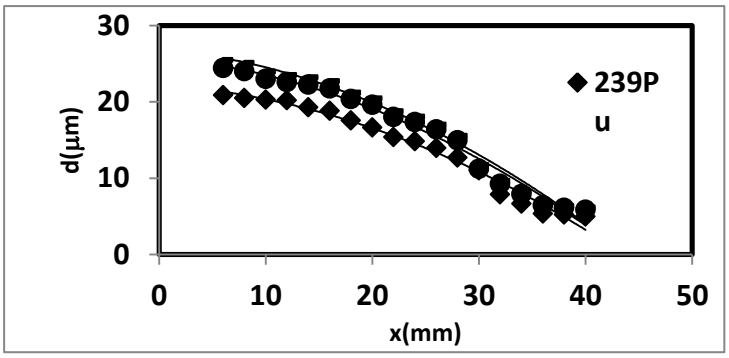

Fig.4 track depth at different source to detector spacing for different alpha emitters.

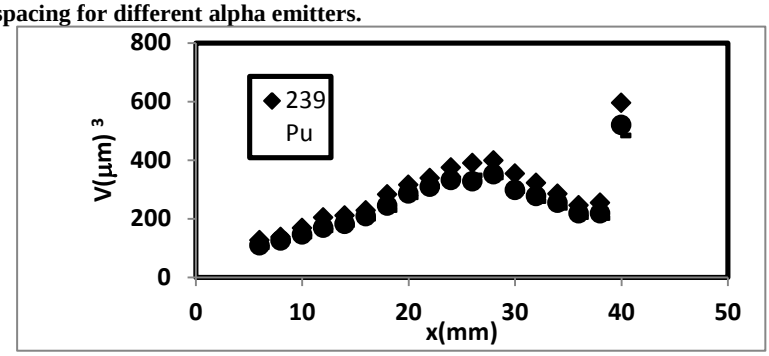

Fig.5 track volume vs source to detector spacing for different alpha emitters.

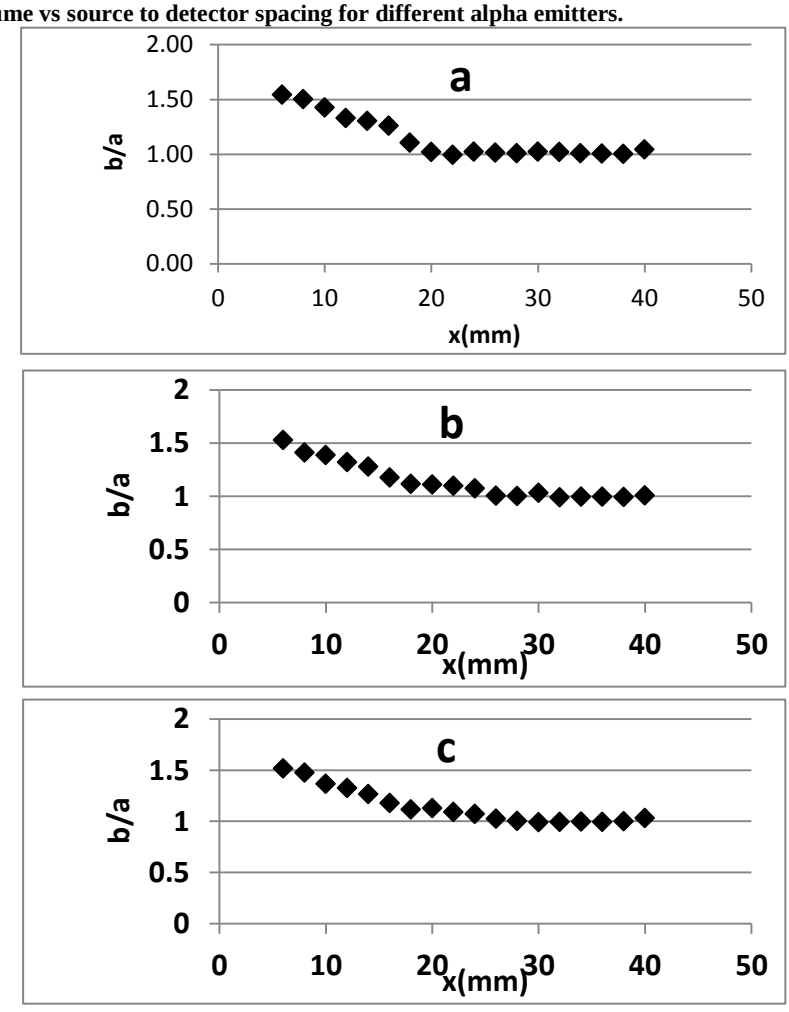

Fig. 6 track major to minor axis ratio at different source to detector spacing (a) for ^{239}Pu, (b) for ^{210}Po and (c) for ^{241}Am.

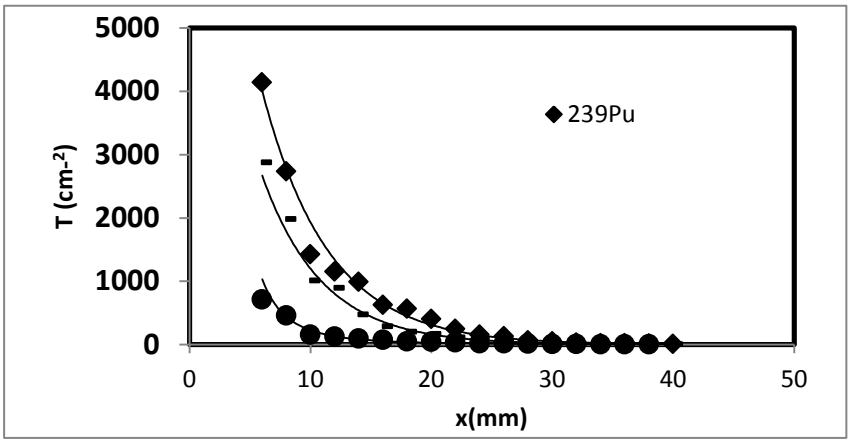

Fig. 7 track density vs source to detector spacing for different alpha emitters .

References:

Ameroa C., J. Golzarria,M. Izerroukenb and G. Espinosaa (2001): ^{148}Gd, ^{238}U, ^{239}Pu and ^{244}Cm alpha particle energy analysis using tracks in solids, Radiation Measurements, vol 34, 341–343.

Bobby R Scott and Raymond A Guilmette (2005): Radiation Toxicology, Ionizing and Nonionizing 601–615, Encyclopedia of Toxicology (Second Edition) Published by Elsevier Inc.

Caresana M. , M. Ferrarini , M. Fuerstner, S. Mayer (2012): Determination of LET in PADC detectors through the measurement of track parameters, Nuclear Instruments and Methods in Physics Research A 683, 8–15

Espinosa G. and R. J. Silva (1998): Transuranic elements alpha-particle energy analysis using nuclear track in solids methodology *Journal of Radioanalytical and Nuclear Chemistry*, *Vol. 234, No 1 2, 283 286.*

Espinosa G. and R. J. Silva (2001): Alpha-particle analysis of a triple isotope ^{239}Pu – ^{241}Am – ^{244}Cm source by nuclear track methodology Journal of Radioanalytical and Nuclear Chemistry, Vol. 248, No. 575–578.

Immèa G.,b, D. Morelli , M. Aranzulla, R. Catalano and G. Mangano (2012): Nuclear track detector characterization for alpha-particle spectroscopy, Radiation Measurements, article in press, 1-5.

Khan AJ., AK. Varshney, R. Parsed, RK. Tyagi and TV. Ramachandran (1990): Calibration of (CR-39) plastic track detector for the measurement of radon and its daughters in dwellings. Nucl Tracks. Radiat Measur. vol 17, 497–502.

Khayrat A. **H. and S. A. Durrani, (1999):** Variation of alpha-particle track diameter in CR-39 as a function of residual energy and etching conditions, Radiation Measurements vol 30, Issue 1, 15-18.

Lounits Z., S. Djeffal. K. Morsli and M. Allab (2001): Track etch parameters in CR-39 detectors for protons and alpha particles of different energies. Nuclear Instruments and Methods in Physics Research B179, 543-550.

Mosier-Bossa P.A., S. Szpak1, F.E. Gordon and L.P.G. Forsley (2009): Characterization of tracks in CR-39 detectors obtained as a result of Pd/D Co-deposition, Eur. Phys. J. Appl. Phys. **46**, 30901.

Ng F.M.F., K.Y. Luk, D. Nikezic, K.N. Yu (2007): Determination of alpha-particle track depths in CR-39 detector from their cross-sections and replica heights, Nuclear Instruments and Methods in Physics Research B 263 , 266–270.

Nikezic **D. , K.N. Yu (2006):** Computer program TRACK_TEST for calculating parameters and plotting profiles for etch pits in nuclear track materials**,** Computer Physics Communications, vol 174, Issue 2, 160–165.

Nikezic D. and K.N. Yu (2003): Calculations of track parameters and plots of track openings and wall profiles in CR39 detector, Radiation Measurements, vol 37, 595 – 601.